Imaging low order CO emission from the $z = 4.12$ QSO PSS 2322+1944

C. L. Carilli
National Radio Astronomy Observatory, P.O. Box O, Socorro, NM, 87801, USA
ccarilli@nrao.edu

P. Cox
Institut d'Astrophysique Spatial, Université de Paris XI, 91405 Orsay, France

F. Bertoldi & K.M. Menten
Max-planck Institut für Radioastronomie, Auf dem Hügel 69, Bonn, D-53121, Germany

A. Omont
Institut d'Astrophysique de Paris, CNRS, 98 bis boulevard Arago, F-75014, Paris, France

S.G. Djorgovski
Astronomy Department, California Institute of Technology, Pasadena, CA, 91125, USA

A. Petric
Astronomy Department, Columbia University, New York, NY USA

A. Beelen
Institut d'Astrophysique Spatial, Université de Paris XI, 91405 Orsay, France

K.G. Isaak
Cavendish Astrophysics, University of Cambridge, Cambridge, UK

R.G. McMahon
Institute of Astronomy, University of Cambridge, Cambridge, UK

ABSTRACT

We present observations of CO 1–0 and CO 2–1 emission from the $z = 4.12$ QSO PSS 2322+1944 using the Very Large Array. The CO emission is extended on a spatial scale of $2''$. This extension could reflect the double nature of the QSO as seen in the optical, or could be diffuse emission with a (redshift corrected) mean brightness temperature of

2.8 K for the CO(2-1) line. We find the CO excitation conditions are lower than in two other IR-luminous $z > 4$ QSOs, suggesting the presence of a significant contribution from cooler, lower density molecular gas ($n(H_2) \sim 5 \times 10^3$ cm^{-3}), although such a conclusion is complicated by the possibility of differential gravitational magnification.

Subject headings: radio continuum: galaxies — infrared: galaxies — galaxies: active, starburst, evolution, radio lines — molecular lines — QSOs

1. Introduction

Two of the more important recent discoveries on nearby galaxies are: (i) the large majority of spheroidal galaxies in the nearby universe contain massive black holes, and (ii) the black hole mass correlates with the mass of the spheroid of the parent galaxy (Richstone et al. 1998; Gebhardt et al. 2000; Ferrarese & Merritt 2000). These discoveries suggest a 'causal connection between the formation and evolution of the black hole and the bulge' (Gebhardt et al. 2000), and have have led to the hypothesis of co-eval formation of massive black holes and galaxy spheroids, perhaps occurring in merging galaxies at high redshift (Franceschini et al. 1999, Blain et al. 1999, Kauffmann & Haenelt 2000; Page et al. 2002). We have undertaken an extensive observational program from radio through (sub)mm wavelengths of high redshift QSOs in order to address the interesting possibility of co-eval black hole and spheroidal galaxy formation (Carilli et al. 2001a, b; Omont et al. 2001, Omont et al. 2002, Carilli, Menten, & Yun 1999; Carilli et al. 2002).

The $z = 4.12$ QSO PSS 2322+1944 has an $M_B = -28.1$, and was discovered in the Digitized Palomar Sky Survey high redshift QSO search (Djorgovski et al. in prep.[1]). Djorgovski et al. (2002) found that 2322+1944 is a double source in the optical, with two similar spectrum components separated by about $1.5''$. This morphology may indicate a QSO pair at $z = 4.12$, or gravitational lensing by an intervening galaxy.

PSS 2322+1944 is the brightest (sub)mm source from the recent surveys of Omont et al. (2002) and Isaak et al. (2002), with a flux density of 9.6 ± 0.5 mJy at 250 GHz and 22.5 ± 2.5 mJy at 350 GHz. The rest frame IR spectral energy distribution (SED) of 2322+1944 is consistent with thermal emission from dust at a temperature of about 47 K (Cox et al. 2002). The apparent FIR luminosity is then 3×10^{13} $L_\odot$. Radio continuum emission from 2322+1944 was detected at 1.4 GHz with the VLA, with a total flux density of 102 ± 20 μJy, and an intrinsic size of about $2''$ (Carilli et al. 2001b).

Cox et al. (2002) show that the radio through IR SED for 2322+1944 is similar to that of the dwarf nuclear starburst galaxy M82, supporting the idea of active star formation co-eval with the AGN activity of the QSO. The implied star formation rate, up to 10^3 $M_\odot$ year^{-1} if the source is not strongly gravitationally lensed, is adequate to form the majority of the stars in a normal spheroidal galaxy in a relatively short time ($\leq 10^8$ years). On the other hand, the global SED for 2322+1944 from cm-to-optical wavelengths is not out of the range defined by lower redshift, lower luminosity QSOs (Carilli et al. 2001b; Sanders et al. 1989), and hence the case for dust-heating by star formation based on the SED alone is by no means secure.

Omont et al. (2001) point out that a pre-requisite for star formation at the rate considered for PSS 2322+1944 is a massive reservoir of molecular gas ($\sim 10^{11}$ $M_\odot$). Such reservoirs have been detected via their CO line emission in other IR-luminous QSOs at $z > 4$ (Omont et al. 1996a; Ohta et al. 1996; Guilloteau et al. 1997, 1999; Carilli et al. 2000; 2002). Recently, Cox et al. (2002) have detected emission in the high order CO transitions from 2322+1944. They find that 2322+1944 has the highest apparent CO(5-4) line luminosity of any $z > 4$ QSO.

In this paper we present observations of CO 1–0 and CO 2–1 emission from the PSS 2322+1944 using the Very Large Array. From these data we derive the spatial distribution and excitation conditions of the molecular gas. We assume $H_o = 65$ km s^{-1} Mpc^{-1}, $\Omega_M = 0.3$ and $\Omega_\Lambda = 0.7$.

2. Observations

PSS 2322+1944 was observed with the VLA in the fall of 2001 using the D configuration (1 km maximum baseline). Observations were made of the redshifted CO 1–0 line at 22.515 GHz, and of the CO 2–1 line at 45.035 GHz. A total of 14 hours was spent on each transition.

The CO 1–0 observations at 22.5 GHz employed the spectral line correlator mode with two polarizations and 7 spectral channels of 6.25 MHz width (= 83 km s^{-1}). Due to limitations with the VLA bandwidth and correlator, the CO 2–1 observations at 45 GHz were done using the continuum correlator mode with two IFs of 50 MHz bandwidth and two polarizations each. One of the IFs was centered on the CO 2–1 emission line, while the second was centered 350 km s^{-1} off the line in order to determine the continuum level, if any. This mode maximizes sensitivity to the line, but sacrifices a measurement of the line velocity profile. Our CO 2–1 analysis will necessarily assume the line profile as given by the 1–0 line.

[1] http://www.astro.caltech.edu/ george/z4.qsos

Standard amplitude and phase calibration were applied, correcting for atmospheric opacity at high frequency, and the absolute flux density scale was set by observing 3C 286. In the analysis below we include a 10% systematic error due to calibration uncertainties at high frequency. Fast switching phase calibration was employed (Carilli & Holdaway 1999) with a cycle time of 3 minutes, although subsequent inspection of the phase stability showed that a cycle time of 15 minutes, or even longer, would have been easily adequate to maintain phase coherence. The observations took place at night under excellent weather conditions, with RMS phase variations after calibration typically less than 10°. The phase coherence was checked by imaging a calibrator with a similar calibration cycle time as that used for the target source. At all times the coherence was found to be better than 90%.

3. Results and Analysis

Figure 1a shows the CO 1–0 emission spectrum from 2322+1944. A Gaussian profile was fit to the spectrum with a resulting full width at half maximum (FWHM) of 200 ± 70 km s^{-1}, a peak flux density of 0.89 ± 0.22 mJy, and a velocity-integrated flux density of 0.19 ± 0.08 Jy km s^{-1}. Zero velocity in Figure 1a is defined as the center of channel 4, corresponding to a heliocentric redshift of 4.11956 for CO 1–0. The Gaussian fit has a central velocity of -22 ± 24 km s^{-1} relative to this redshift, corresponding to a redshift of 4.1192 ± 0.0004. For comparison, the Gaussian fit to the CO(5-4) line has a FWHM = 273 ± 50 km s^{-1}, and a central redshift of 4.1199 ± 0.0008 (Cox et al. 2002).

The image of the CO 1–0 emission averaged over channels 3, 4, and 5 is shown in Figure 1b, and the average of the continuum channels (1 and 6) is shown in Figure 1c. The source is spatially unresolved, with an upper limit to the (deconvolved) source size of 3″ (derived from Gaussian fitting), and a peak flux density of 0.65 ± 0.07 mJy (note that this peak corresponds to the average of channels 3, 4, and 5). The upper limit (2σ) to continuum emission at 22 GHz is 0.14 mJy.

Figure 2a shows the integrated CO 2–1 emission from 2322+1944, while 2b shows the continuum channel. No continuum emission is detected to a 2σ limit of 0.15 mJy. The CO emission is resolved spatially. A Gaussian fit results in a deconvolved source size of FWHM = $2.1'' \times 1.6''$ with a major axis position angle of 152°, and a total flux density of 2.7 ± 0.24 mJy. The implied (redshift corrected) mean brightness temperature is 2.8 K. The velocity-integrated flux density is 0.92 ± 30 Jy km s^{-1}, assuming a line width as given by the CO 1–0 transition. The CO 2–1 image also shows emission extending about 2″ to the southwest of the peak position. This structure repeats (to within the noise) on the three different observing days. The average (redshift corrected) brightness temperature of this emission is 0.5 ± 0.1 K. We note that the observed morphology of the CO 2–1 emission agrees within the errors with that observed for the radio continuum emission at 1.4 GHz (Carilli et al. 2001b).

The data for the velocity-integrated flux densities for various CO transitions for 2322+1944 are plotted in Figure 3. The higher order transition data is taken from Cox et al. (2002). Also plotted are the corresponding numbers for two other IR-luminous QSOs at $z > 4$, BRI 1202–0725 at $z = 4.7$ and BRI 1335–0417 at $z = 4.4$, for which multiple CO transitions have been observed (see Carilli et al. 2002; Cox et al. 2002). The data have been normalized to the velocity-integrated line flux density for CO(5-4). For comparison, we have included the CO ladder observed for the best studied nuclear starburst galaxy M82 (Güsten et al. 1993; Mao et al. 2000), and that for the integrated emission from the Milky Way disk inside the solar radius (excluding the Galactic center) as seen by COBE (Fixsen, Bennett, & Mather 1999).

We have fit a standard one component LVG model simulating a spherical cloud to interpret the observed line ratios (for details see Carilli et al. 2002). Due to the lack of constraints, there is a degeneracy in LVG modeling between various parameters such as the density and kinetic temperature (Güsten et al. 1993). Our modeling is not meant as an exhaustive analysis, but is merely representative of the types of conditions that can give rise to the observed line ratios. Given the paucity of information, we adopt a kinetic temperature of 47 K, corresponding to the temperature derived from the far-IR spectrum of thermal emission by warm dust (Cox et al. 2002). We also use the cosmic microwave background radiation temperature at $z = 4.12$ of 14 K. The CO data can be reasonably fit by a model with: N(CO) = 2×10^{19} cm^{-2}, n(H_2) = 5×10^3 cm^{-3}, and grad $V = 1$ km s^{-1} pc^{-1}. Given the inhomogeneity of the interstellar medium in the Milky Way and nearby galaxies, our assumption of uniform physical conditions is crude but appropriate

for a source with four detected lines from the main CO species and no information on rare isotopomers.

4. Discussion

The optical QSO positions are shown as crosses on Figure 2a. The deconvolved size and position angle of the CO 2–1 emission from PSS 2322+1944 are consistent with the separation and position angle of the double optical QSO components found by Djorgovski et al. (2002), as is the observed radio continuum morphology at 1.4 GHz (Carilli et al. 2001). However, the resolution of the current VLA image is insufficient to determine if the CO emission is from two small components associated with the optical QSOs, or from more diffuse emission with a mean (redshift corrected) brightness temperature of 2.8 K. The more extended emission to the southwest appears to be robust, although, given the relatively low surface brightness, we feel this extension needs to be confirmed with further observations.

As discussed in Carilli et al. (2002), the CO excitation conditions for two other IR-luminous QSOs at $z > 4$, BRI 1202–0725 and BRI 1335–0417, are similar to those seen in the dwarf nuclear starburst galaxy M82, and are consistent with a fairly high kinetic temperature of 70 K and a high (mean) molecular gas density of 2×10^4 cm^{-3}. For 2322+1944 we find excitation conditions intermediate between those seen in M82 and those seen for the disk of the Milky Way. The data are consistent with a kinetic temperature equal to the temperature derived from the far-IR SED of the thermal emission by warm dust (47 K), and a density for the molecular gas of n(H_2) = 5×10^3 cm^{-3}, ie. a factor 4 lower than that found for 1202–0725 and 1335-0417. These results may indicate that the CO emission from 2322+1944 is dominated by gas that is more diffuse and cooler than is seen in the other two QSOs. However, if the CO emission from 2322+1944 is strongly lensed, then differential magnification due to (possibly) different source-plane spatial distributions for the low and high excitation molecular gas makes a detailed excitation analysis problematic until higher resolution observations, and a proper lens model, are available.

The apparent CO 1–0 luminosity, L', for PSS 2322+1944 is 1.5×10^{11} K km s^{-1} pc^2. The H_2 gas mass can be calculated from the CO luminosity assuming a value of X = the H_2 mass-to-CO(1-0) luminosity conversion factor in M$_\odot$ (K km s^{-1} pc^2)$^{-1}$ (Solomon et al. 1997). We adopt a value of X $\simeq$ 0.8, as found for Ultra-Luminous Infrared Galaxies ($L_{FIR} \sim 10^{12}$ L$_\odot$; ULIRGs) by Downes and Solomon (1998), leading to a molecular gas mass of 1.2×10^{11} M$_\odot$. Of course, X depends on a number of factors, including the excitation conditions, and in the case of 2322+1944 the possibility of gravitational lensing complicates the situation.

Lastly, we consider the continuum-to-line ratio: $[L_{\rm FIR}]/[L'_{\rm CO(1-0)}]$, in units of L$_\odot$ (K km s^{-1} pc^2)$^{-1}$. Solomon et al. (1997) show that this ratio increases with increasing $L_{\rm FIR}$, with values between 5 and 50 for Galactic Giant Molecular Clouds and nearby galaxies with $L_{\rm FIR} \leq 10^{10}$ L$_\odot$, and values between 80 and 250 for ULIRGs. Evans et al. (2001) have extended this relationship to include IR-excess, optically selected QSOs at $z \leq 0.17$. These QSOs have $L_{\rm FIR}$ values ranging from a few $\times 10^{11}$ L$_\odot$ to 10^{12} L$_\odot$. They find that the low z QSOs typically show continuum-to-line ratios (as defined above) between 100 and 260, with the majority of sources toward the low end of this range. [Note that we have converted from their $L_{\rm IR}$ to $L_{\rm FIR}$ using a ratio of 0.52, as found by Dale et al. (2000) for a large sample IR-selected galaxies.] Evans et al. (2001) also find that the QSOs with high continuum-to-line ratios reside in optically disturbed galaxies, ie. on-going mergers of gas rich spiral galaxies, while the sources with low values reside in more normal-looking galaxies.

For 2322+1944 we find: $[L_{\rm FIR}]/[L'_{\rm CO(1-0)}] = 200$ L$_\odot$ (K km s^{-1} pc^2)$^{-1}$. For comparison, in BRI 1335–0417 and BRI 1202–0725 values of about 340 were found by Carilli et al. (2002). Carilli et al. argued that the large continuum-to-line ratio in these latter two QSOs, both of which have $L_{FIR} \geq 10^{13}$ L$_\odot$, continues the trend of increasing continuum-to-line ratio with increasing IR luminosity. The fact that 2322+1944 has a continuum-to-line ratio more consistent with ULIRGs, and with low redshift, lower IR luminosity QSOs, could be used to argue for strong (factor ~ 10) gravitational magnification of the emission regions, thereby lowering its IR luminosity to $\sim 10^{12}$ L$_\odot$. However, given the scatter in the relationship between IR luminosity and the continuum-to-line ratio, this is at best a weak argument in favor of gravitational lensing.

Detecting the massive reservoir of molecular gas in PSS 2322+1944 is one of the required (although not sufficient) elements for demonstrating the existence of

active star formation co-eval with the AGN activity in this high-z QSO. However, the possibility of gravitational lensing in PSS 2322+1944 complicates the physical analysis. An argument in favor of lensing is the relatively low velocity dispersion for the CO emission. The observed value of 200 km s^{-1} is typical for a galaxy potential, but is low for a group potential, as might be expected if the observed CO line was the sum of emission from the host galaxies of a QSO pair at $z = 4.12$. If the system is strongly gravitationally lensed, then judicious use of a lens model could elucidate structure in the source plane on finer physical scales (≤ 100 pc) than can be obtained normally (Yun et al. 1997; Lewis et al. 2002). Sensitive, high resolution observations of the CO 2–1 emission from 2322+1944 are planned to confirm, and better resolve, the molecular line emitting regions, while observations of higher order transitions at high spatial resolution are planned to better constrain the CO excitation conditions.

The National Radio Astronomy Observatory (NRAO) is operated by Associated Universities, Inc. under a cooperative agreement with the National Science Foundation. SDG acknowledges partial support from the Bressler Foundation. We thank A. Mahabel for assistance with the optical astrometry, and the referee, A. Evans, for very helpful comments.

REFERENCES

Blain, A.W. Jameson, A., Smail, I., Longair, M.S., Kneib, J.-P., & Ivison, R.J. 1999, MNRAS, 309, 715

Carilli, C. L. & Holdaway, M. A. 1999, Radio Science, 34, 817

Carilli, C.L., Bertoldi, F., Rupen, M.P. et al. 2001a, ApJ, 555, 625

Carilli, C.L., Bertoldi, F., Omont, A., Cox, P., McMahon, R.G., & Isaak, K. 2001b, AJ, 122, 1679

Carilli, C.L., Menten, K.M., & Yun, M.S. 1999, ApJ, 521, L25

Carilli, C.L., Kohno, K, Kawabe, K. et al. 2002, AJ, in press

Cox, P., Omont, A., Djorgovski, G., Bertoldi, F. et al. 2002, A & A (letters), submitted

Dale, D.A., Helou, G., Contursi, A., Silberman, M., & Kolhatkar, S. 2001, ApJ, 549, 215

Downes, D., & Solomon, P.M. 1998, ApJ, 507, 615

Djorgovski, S.G. et al. 2002, ApJ, submitted

Evans, A.S., Frayer, D.T., Surace, J.A., & Sanders, D.B. 2001, AJ, 121, 1893

Ferrarese, L. & Merritt, D. 2000, ApJ (letters), 539, 9

Fixsen, D.J., Bennett, C.L., & Mather, J.C. 1999, ApJ, 526, 207

Franceschini, A., Hasinger, G., Mayaji, T., & Malquori, D. 1999, MNRAS (letters), 310, 5

Gebhardt, Karl et al. 2000, ApJ (letters), 539, 13

Guilloteau, S., Omont,A., McMahon, R.G., Cox,P., & Petitjean, P. 1997, A&A, 328, L1

Guilloteau, S., Omont, A., Cox, P., McMahon, R. G., & Petitjean, P. 1999, A&A, 349, 363

Güsten, R., Serabyn, E., Kasemann, C., Schinckel, A., Schneider, G., Schulz, A., & Young, K. 1993, ApJ, 402, 537

Kauffmann, G. & Haehnelt, M. 2000, MNRAS, 311, 576

Lewis, G.F., Carilli, C.L., Papadopoulos, P. Ivision R.J. 2002, MNRAS, 330, L15

Mao, R.Q., Henkel, C., Schulz, A. et al. 2000, A& A 358, 433

Ohta, Kouji, Yamada, T., Nakanishi, K., Kohno, K., Akiyama, M., & Kawabe, R. 1996, Nature, 382, 426

Omont, A., McMahon, R. G., Cox, P., Kreysa, E., Bergeron, J., Pajot, F., & Storrie-Lombardi, L.J. 1996a, A&A, 315, 1

Omont, A., Petitjean, P., Guilloteau, S., McMahon, R. G., Solomon, P. M., & Pecontal, E. 1996b, Nature, 382, 428

Omont, A., Cox, P.; Bertoldi, F., McMahon, R. G., Carilli, C., & Isaak, K. G 2001, A& A, 374, 371

Page, M.J., Stevens, J.A., Mittaz, J., Carrera, F.J. 2002, Science, 294, 2516

Richstone, D., Ajhar, E. A., Bender, R. et al. 1998, Nat. Supp., 395A, 14

Sanders, D.B., Phinney, E. S., Neugebauer, G., Soifer, B. T., & Matthews, K. 1989, ApJ, 347, 29

Solomon, P.M., Downes, D., Radford, S., & Barrett, J.W. 1997, ApJ, 478, 144

Yun, M.S., Scoville, N. Z., Carrasco, J. J., & Blandford, R. D. 1997, ApJ, 479, L9

This 2-column preprint was prepared with the AAS LaTeX macros v4.0.

Figure Captions

FIG. **1a**.— The CO 1–0 spectrum of PSS 2322+1944 as measured at 22.515 GHz at a spatial resolution of 3.8″. Zero velocity is defined as the center of channel 4, corresponding to a heliocentric redshift of 4.11956 for CO 1–0. Each channel is 83 km s^{-1} wide, and the rms noise in each channel is 0.12 mJy $beam^{-1}$. The dashed line is a Gaussian fit to the velocity profile (see section 3).

1b. The contour image of the average of channels 3, 4, and 5 from the spectrum shown in Figure 1a. The contour levels are: -0.24, -0.12, 0.12, 0.24, 0.36, 0.48, 0.60 mJy $beam^{-1}$. The Gaussian restoring CLEAN beam has FWHM = 3.9″ × 3.7″ with a major axis position angle of -46°, as shown in the inset. The rms noise on this image is 74μJy $beam^{-1}$. The crosses in this and subsequent images show the position of the two optical QSOs found by Djorgovski et al. (2002)

1c. The contour image of the off-line channels (1 and 6) from the spectrum shown in Figure 1a. The contour levels and beam are the same as Figure 1b.

FIG. **2a**.—The contour image of the average of the on-line IF for the CO 2–1 observations of PSS 2322+1944. The IF bandwidth is 50 MHz (= 350 km s^{-1}), and is centered at 45.035 GHz, corresponding to a heliocentric redshift of 4.1191 GHz for CO 2–1. The contour levels are -0.24, -0.12, 0.12, 0.24, 0.36, 0.48, 0.60 mJy $beam^{-1}$. The Gaussian restoring CLEAN beam has FWHM = 1.8″ × 1.4″ with a major axis position angle of -28°, as shown in the inset. The rms noise on this image is 77μJy $beam^{-1}$.

2b. The contour image of the off-line IF for the 44.985 GHz VLA observations of 2322+1944. The contour levels and beam are the same as Figure 2a.

FIG. **3**. — The velocity-integrated flux densities for CO emission from PSS 2322+1944, as derived from data from this paper and from Cox et al. (2002), are show as large filled circles with error bars. Also plotted are the corresponding values for the QSOs BRI 1202–0725 at $z = 4.7$ (open squares), and BRI 1335–0417 at $z = 4.4$ (open triangles) (from Carilli et al. 2002). The solid triangles are the data for the CO ladder for the integrated emission from the Milky Way disk inside the solar radius (excluding the Galactic center) as seen by COBE (Fixsen, Bennett, & Mather 1999). The open circles are the results for the starburst nucleus of M82 (Güsten et al. 1993; Mao et al. 2000). The ordinate is the velocity-integrated line flux density. The CO(5-4) line has been detected in all the sources, and the velocity-integrated line flux densities for the other transitions in each source have all been normalized by the corresponding CO(5-4) values, except for the Milky Way, for which the values are normalized at CO(3-2). The short dash line shows an LVG model with $T_{kin} = 47$ K and $n(H_2) = 5 \times 10^3$ cm^{-3}.

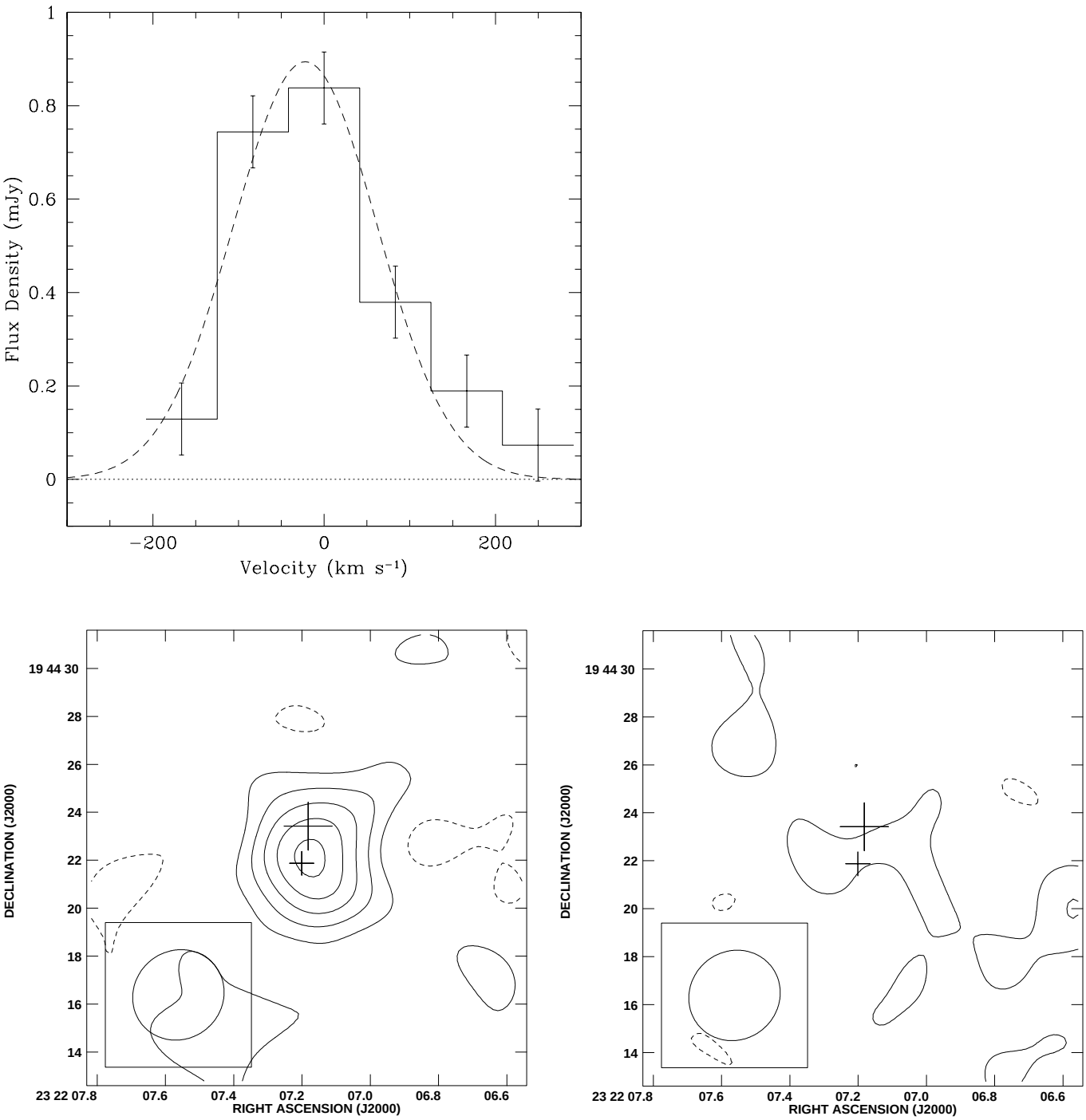

Fig. 1.— 1a – upper; 1b – lower left; 1c – lower right

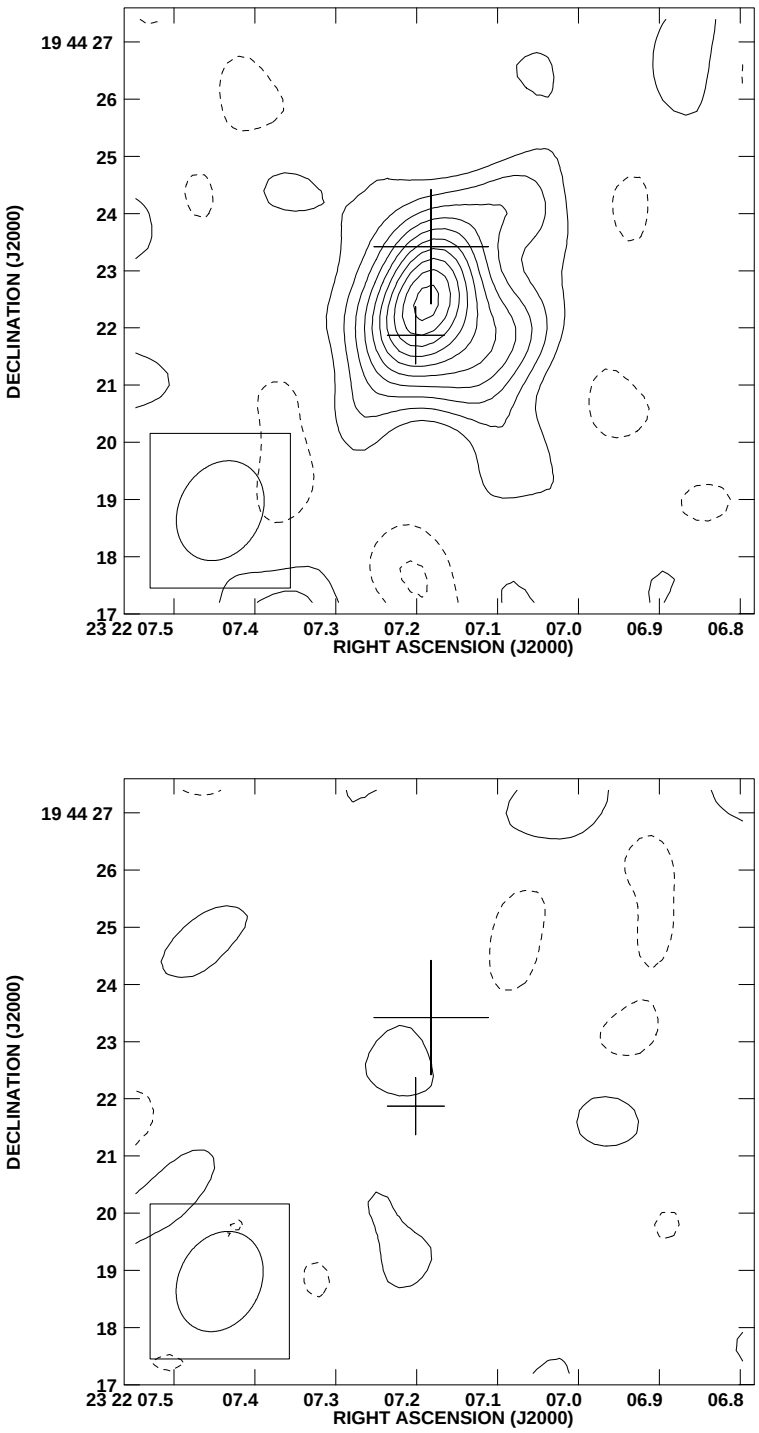

Fig. 2.— 2a – upper; 2b – lower

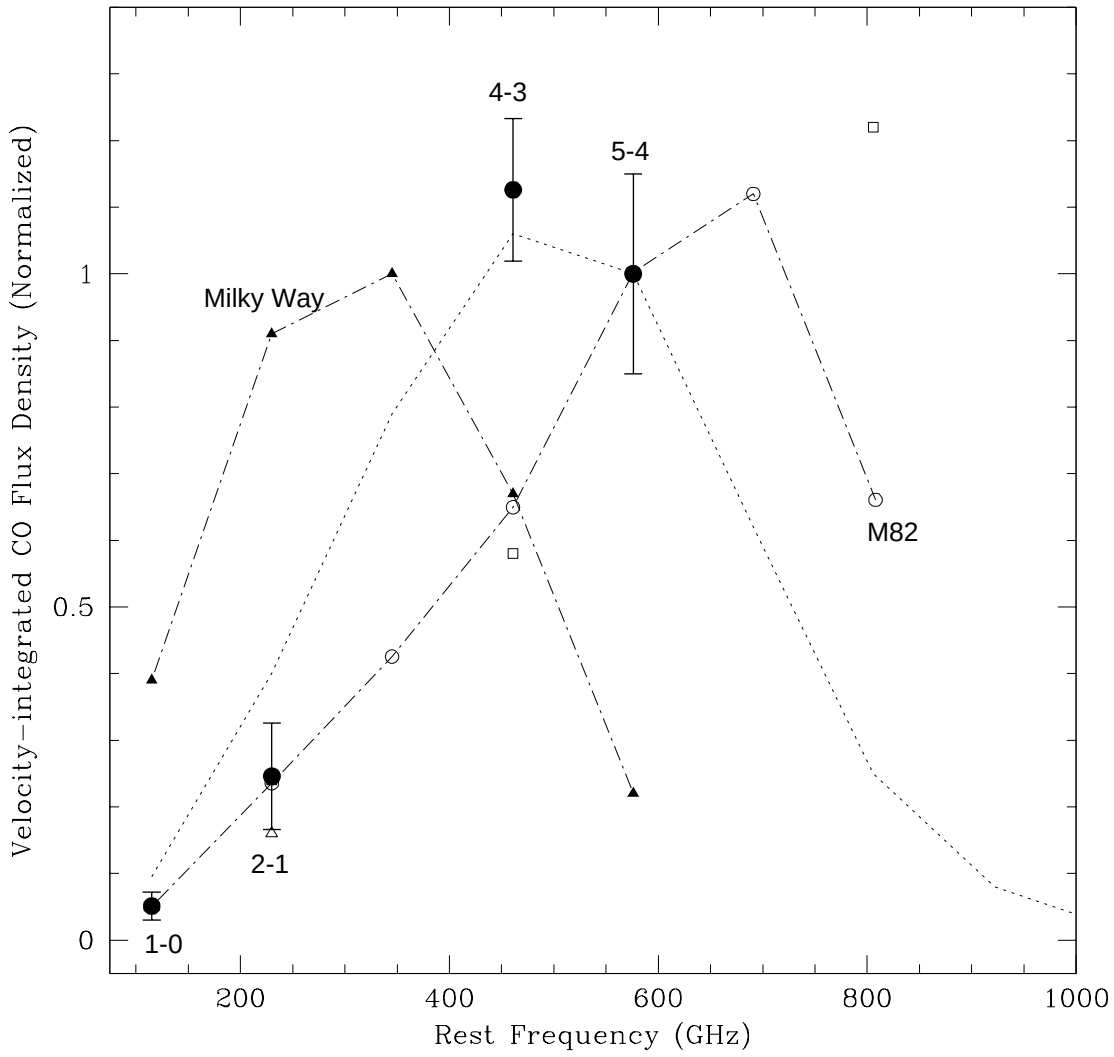
4-3
5-4
Milky Way
M82
2-1
1-0
Velocity−integrated CO Flux Density (Normalized)
Rest Frequency (GHz)
0
0.5
1
200
400
600
800
1000

Fig. 3.—